Journal of Alloys and Compounds 509 (2011) 8584–8589

Contents lists available at ScienceDirect

Journal of Alloys and Compounds

journal homepage: www.elsevier.com/locate/jallcom

Electrical conduction and dielectric relaxation process in $Ce_{0.8}Y_{0.2}O_{1.9}$ electrolyte system

K.P. Padmasree[a,*], R.A. Montalvo-Lozano[b], S.M. Montemayor[b], A.F. Fuentes[a]

[a] Cinvestav Unidad Saltillo, Apartado Postal 663, 25000 Saltillo, Coahuila, Mexico
[b] Facultad de Ciencias Químicas, Universidad Autónoma de Coahuila, Bvd. Venustiano Carranza s/n, 25280 Saltillo, Coahuila, Mexico

HIGHLIGHTS

- We present conductivity and dielectric relaxation of Ce0.8Y0.2O1.9 electrolyte.
- Ac conductivity obeys the universal dielectric response at low temperatures.
- Two relaxation peaks were observed in the tan delta spectra.
- The migration energy EM and the dissociation energy EO are estimated.
- Sums of these values are equal to activation energy obtained from conductivity plot.

ARTICLE INFO

Article history:
Received 24 November 2010
Received in revised form 9 June 2011
Accepted 13 June 2011
Available online 17 June 2011

Keywords:
Conductivity
Dielectric
Oxides
Electrolyte
Ceramics

ABSTRACT

In this work, we present the electrical conductivity and dielectric relaxation studies of 20 mol% yttria doped ceria ($Ce_{0.8}Y_{0.2}O_{1.9}$) electrolyte prepared by mechanical milling technique. The ac conductivity was found to obey the universal dielectric response at low temperatures. At high temperatures, the conductivity value estimated from the high frequency plateau agreed with the bulk conductivity (σ_b) obtained form the impedance spectra and the low frequency plateau value agreed with the grain boundary conductivity (σ_{gb}). Temperature dependence of σ_b and σ_{gb} gives the activation energies for conduction in the bulk and grain boundary. Two relaxation peaks were observed in the tan delta spectra; the high frequency relaxation peak is due to the bulk conduction and the low frequency peak result from the grain boundary conduction. The migration energy E_M and the energy required for the creation of free oxygen vacancies assisting oxide ion migration E_O is estimated from the resonant frequency and maxima of the tan delta spectra of these relaxation peaks. The sums of these two values in the low and high frequency peaks are nearly equal to the activation energies obtained from the bulk and grain boundary conductivity plot.

1. Introduction

Solid electrolytes with high oxygen ion conductivity have been attracting great interest owing to their applications in solid oxide fuel cells, oxygen sensors, oxygen pumps and oxygen-permeable membranes with high economic and environmental benefits [1–3]. To be technologically workable, these oxide electrolytes must exhibit high oxide ion mobility at low temperatures. The ionic conductivity of oxide ion conductors varies with the addition of aliovalent dopant cations. Fluorite oxides so doped become good oxygen ion conductors because of the introduction of oxygen vacancies to maintain charge balance [4]. Doped ceria electrolytes have greater ion conductivity at low temperatures compared to conventional yttria stabilized zirconia (YSZ) [5]. The diffusion of oxygen ions via oxygen vacancies is the main electric conduction process in these oxides. The ionic displacements result in a dipole moment which involves a dielectric relaxation process due to the migration of O^{2-} ions [6].

Materials which contain both conductive and dielectric (insulating) phases are observed in a wide range of systems including ceramics, polymers and composites. These systems display a very similar frequency dependent conductivity and permittivity, often referred as Jonscher's 'Universal Dielectric Response' (UDR) [7]. It explains that the ac conductivity, $\sigma(\omega)$ is frequency independent at low frequencies, but increases with increase in frequencies following the power law behavior, $\sigma(\omega)\alpha\ \omega^n$. The overall response can be given by

$$\sigma(\omega) = \sigma_0 + A\omega^n \quad (1)$$

* Corresponding author. Tel.: +52 8444389612; fax: +52 8444389610.
E-mail address: padma512@yahoo.com (K.P. Padmasree).

0925-8388/$ – see front matter © 2011 Elsevier B.V. All rights reserved.
doi:10.1016/j.jallcom.2011.06.036

where ω is the angular frequency, A is a constant and n is the power law exponent, $0 \leq n \leq 1$, which has been linked to the correlation effects in the dynamics of hopping ions. The dielectric relaxation technique is a widely used method, which measures the dissipation of electrical energy, or the tangent of the loss angle ($tan\,\delta$) due to the electric field induced reorientation of defects, where $tan\,\delta$ ($=\varepsilon''/\varepsilon''$) corresponds to the dissipation factor and the angle δ is the phase difference between the applied field and induced current. The complex impedance (Z^*) data were converted into the complex permittivity (ε^*) by the relation,

$$\varepsilon^* = \frac{1}{j\omega C_0 Z^*} = \varepsilon' - j\varepsilon'' \quad (2)$$

$$\varepsilon' = \frac{-Z''}{\omega C_0 (Z'^2 + Z''^2)}, \qquad \varepsilon'' = \frac{Z'}{\omega C_0 (Z'^2 + Z''^2)} \quad (3)$$

where $C_0 = \varepsilon_0 A/t$, is the vacuum capacitance, t is the thickness of the sample, A is the effective area of the electrodes, ε_o is the permittivity of free space (8.854×10^{-14} F/cm), $j = \sqrt{-1}$, ε' is the dielectric constant and ε'' is the dielectric loss which is nothing but the energy dissipation in the material with the ac field, Z' and Z'' are the real and imaginary part of the impedance, respectively. The dielectric experiments directly provide the important knowledge of relaxation process due to ionic displacement induced by the migration of O^{2-} ions. The activation energy for ionic conduction is the sum of migration energy per oxide ion, E_M and the energy required for the creation of mobile free oxygen vacancy which assists O^{2-} migration, E_O. The oxide ion diffusion involves various thermal activation processes and the activation energy estimated from the electrical conductivity does not separate such processes and the obtained information is insufficient to estimate the value of E_M and E_O. Temperature dependence of the dielectric relaxation process provide the value of E_M and E_O, and this procedure has been used in ion conducting oxide systems and polaronic conductions in strongly correlated electrons system [8–14]. The resonance frequency of the relaxation process due to O^{2-} movement within the bulk and the grain boundary are different. The dielectric relaxation process has been applied to many oxide electrolytes [15–17], however there has been a few reports relating the estimation of E_M and E_O from the dielectric measurements in the fluorite oxides. The fluorite structured ceria when doped with a trivalent cation, Y^{3+} in the present case; one oxygen vacancy is formed for every two trivalent cations for charge neutrality and is represented by the Kröger–Vink notation as:

$$Y_2O_3 + 2CeO_2 \rightarrow 2Y'_{Ce} + 3O_o^x + V_o^{\bullet\bullet} \quad (4)$$

where Y'_{Ce} indicates one Ce^{4+} site occupied by one Y^{3+} ion. The oxygen vacancy $V_o^{\bullet\bullet}$ occupies one of the eight equivalent sites in the cubic structure and gives rise to reorientation relaxation process. In the present study, $Ce_{0.8}Y_{0.2}O_{1.9}$ electrolyte has been synthesized by mechanical milling process, and the electric and dielectric properties have been investigated.

2. Experimental procedure

Powder sample of $Ce_{0.8}Y_{0.2}O_{1.9}$ was synthesized by mechanical milling, using high purity (Aldrich, >99+%) CeO_2 and Y_2O_3 as starting materials. Stoichiometric mixtures of the above chemicals were placed in zirconia containers together with 20 mm diameter zirconia balls as grinding media (balls to powder mass ratio = 10:1). Dry mechanical milling was carried out in air in a planetary ball mill by using a rotating disc speed of 350 rpm. Phase evolution on milling was analyzed by using X-ray powder diffraction in Philips X'pert diffractometer using Ni-filtered CuKα radiation (λ = 1.5418 Å). The relative density of the sintered sample was measured by the Archimedes method. The experimental method most frequently used for measuring the electrical and dielectric characteristics is the complex impedance method, and is used almost exclusively in the area of ionic conduction in solids. Specimens for electrical property measurements were pellets obtained by pressing the sample powder in a hydraulic press at a pressure of 5 MPa with a diameter of 10 mm diameter and ~1 mm thickness, and sintered at 1500 °C for 5 h, The two electrodes were formed by applying platinum paste (SPI supplies Brand platinum paint) to either surface of the pellets and then heat treated at 600 °C for 2 h before the measurement to burn out the binder of the platinum paste and to ensure good contact of the electrodes with the pellet. The transport properties of the sintered pellets were examined by ac impedance spectroscopy over a temperature range from 140 to 360 °C and frequency range from 100 Hz to 1 MHz using Solartron 1260 Frequency Response Analyzer.

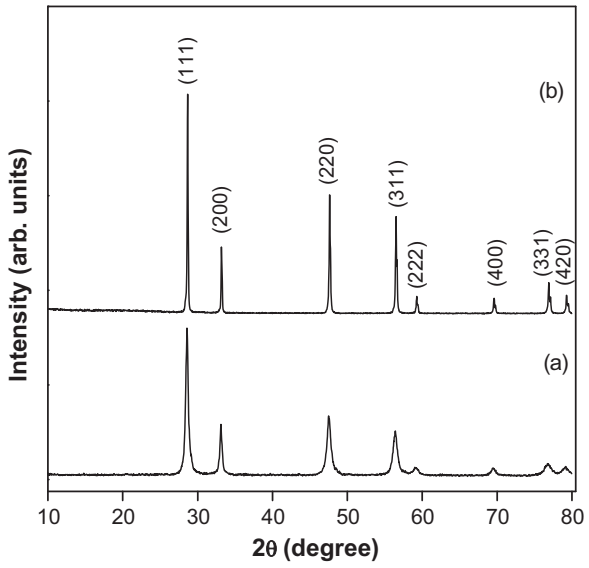

Fig. 1. XRD pattern obtained for $Ce_{0.8}Y_{0.2}O_{1.9}$ after (a) 1 h milling and (b) sintered at 1500 °C.

3. Results and discussion

Fig. 1 shows the powder X-ray diffraction patterns of $Ce_{0.8}Y_{0.2}O_{1.9}$ sample obtained after 1 h milling (a) and sintered at 1500 °C for 5 h (b). The X-ray diffraction pattern confirms the formation of single phase cubic fluorite structure after 1 h milling. Any additional phase corresponding to yttria is not observed and it ensures the complete dissolution of the dopant into CeO_2 lattice. XRD pattern of the sintered sample is same as that of the green sample except the XRD peaks are more intense. This implies that the sintering process helps to increase the crystal size and the increase of pellet compaction. The crystallite size (D) of the sintered powder was calculated to be 98.4 nm using the Scherrer formula, $D = 0.9\lambda/\beta\cos\theta$, where λ is the wave length of x-rays, β is the corrected half width line corresponding to the (1 1 1) plane, θ is the corresponding diffraction angle. The lattice parameter 'a' was calculated to be 0.5408 nm using the relation, $a = d\sqrt{h^2 + k^2 + l^2}$ where d ($= \lambda/2\sin\theta$) is the planar spacing [18]. The relative density of the sample sintered at 1500 °C is 97% of theoretical density and it indicates that highly sinterable samples can be synthesized by mechanical milling. Fig. 2 shows the complex impedance analysis conducted at 300 °C, where the real part (Z') of the total impedance is plotted against the imaginary part (Z'') as a parametric function of frequency. In an ideal case, the ac impedance of an ionic conductor contains the contributions from the bulk, grain boundaries and the electrode–electrolyte interface, which can be reflected in a complex impedance plot by three successive semicircles, representing different relaxation processes. The three contributions can be observed in Fig. 2. The typical equivalent electrical circuit for such impedance plot consists of parallel combination of resistance and capacitance (R–C) blocks connected in series. The real axis intercept of the high frequency arc represents the bulk resistance (R_b), the intercept of the intermediate frequency arc is the grain boundary resistance (R_{gb}) and the polarization effects from charge carriers blocking at the electrodes are seen at the low frequencies.

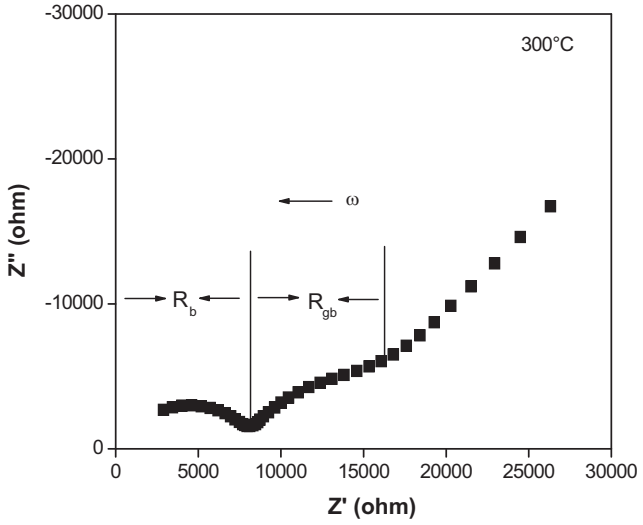

Fig. 2. Complex impedance plots for $Ce_{0.8}Y_{0.2}O_{1.9}$ electrolyte at 300 °C.

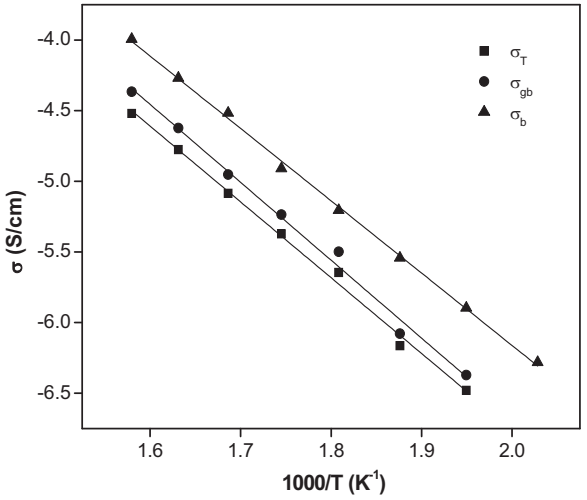

Fig. 3. Arrhenius plots of bulk, grain boundary and total conductivity of $Ce_{0.8}Y_{0.2}O_{1.9}$ electrolyte.

The depressed semicircular patterns have its centers below the real axis of the impedance plot. It gives rise to a depression angle (θ), i.e., the angle between the real impedance axes and the centre of the semicircle. This depression angle becomes the measure of a depression parameter, α where $\alpha = 2\theta/\pi$ [7]. The value of α ranges between 0 and 1, depending on Debye or non-Debye like relaxation of the material. Thus for ideal Debye like behavior $\theta \rightarrow 0^\circ$ or $\alpha \rightarrow 0$ and an extreme non-Debye response can be visualized as $\theta \rightarrow 90^\circ$ or $\alpha \rightarrow 1$. The θ value obtained at 300 °C is about 24.3° and 34.7° and calculated α values are 0.27 and 0.38 for the high frequency and intermediate frequency arcs. This indicates that both bulk and grain boundary relaxation processes are non-Debye type with a distribution of relaxation times. The degree of distribution of relaxation time is broad in the grain boundary compared with that of the bulk. In the grain boundary, a large deviation has been expected because there are various migration paths of O^{2-} ions across the boundary and each migration path has a relaxation time peculiar to it [19]. The temperature dependence of the conductivity is obtained from the impedance analysis. Fig. 3 shows the plot of $\log\sigma$ vs $1000/T$ for the bulk, grain boundary and total conductivities of $Ce_{0.8}Y_{0.2}O_{1.9}$ sample. It follow Arrhenius type law of the form, $\sigma = \sigma_o \exp\ (-E_a/kT)$, where σ_o is the pre-exponential factor which is related to the effective number of mobile oxygen ions and E_a denotes the activation energy for the ion conduction process. The activation energy is calculated from the slope of $\log\sigma$ vs $1000/T$ plot and the values of conductivities and activation energies are listed in Table 1.

Fig. 4 shows the ac conductivity spectra as a function of log f at various temperatures. The conductivity plots strongly depend on the measuring temperatures. From the figure we can see in the low temperature range, there are only one plateau region and a high frequency dispersion following the power law exponent [7]. The frequency dispersion at high frequencies shifts to higher frequencies with increase of temperature. The temperature range at and above 240 °C showed two plateaus, which are frequency independent in the low and high frequency region. The appearance of low frequency plateau is due to the blocking effect of grain boundaries

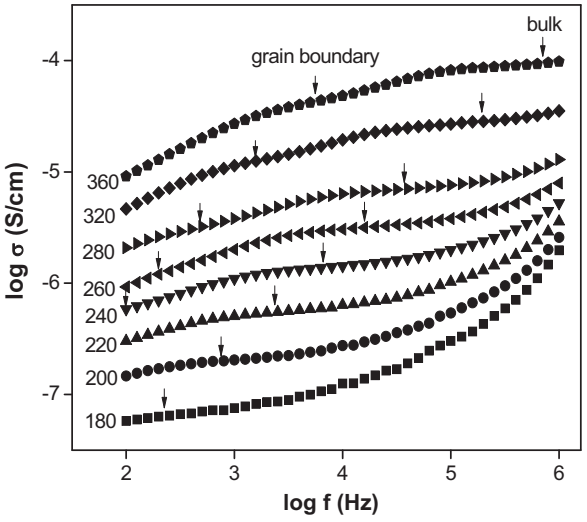

Fig. 4. Frequency dependent conductivity spectra at different temperatures (°C).

which show prominent effect at low frequencies. In the temperature range from 240 to 360 °C, the conductivity value estimated from the low frequency plateau did not agree with that of bulk conductivity, but agreed with the conductivity estimated from the grain boundary of the impedance spectra. The conductivity dispersion in the intermediate frequency range is high for the material having higher grain boundary resistivity than the bulk resistivity [20]. So we can assume that the plateau in the low frequency range for the temperatures from 240 to 360 °C is due to the polarization of space charge due to the presence of large grain-boundary barrier. This means that one part of the mobile oxide-ions contributes to oxide ion conduction and the other part does to the polarization at the grain boundary barrier as the space charge. But in the high frequency range, the charge can follow no longer with the frequency; the plateau at the high frequency corresponds to bulk conductiv-

Table 1
Various conductivity data obtained at 633K for $Ce_{0.8}Y_{0.2}O_{1.9}$; σ_b, σ_{gb}, σ_T are the bulk, grain boundary and total conductivity obtained from the impedance spectra, σ_{ach} and σ_{acl} are the ac conductivity value estimated from the high and low frequency plateau region and E_b, E_{gb} and E_T are the respective activation energy values.

Compound	σ_b (S/cm)	σ_{gb} (S/cm)	σ_T (S/cm)	σ_{ach} (S/cm)	σ_{acl} (S/cm)	E_b (eV)	E_{gb} (eV)	E_T (eV)
$Ce_{0.8}Y_{0.2}O_{1.9}$	8.8×10^{-5}	4.9×10^{-5}	3.2×10^{-5}	8.8×10^{-5}	4.8×10^{-5}	1.05	1.09	1.06

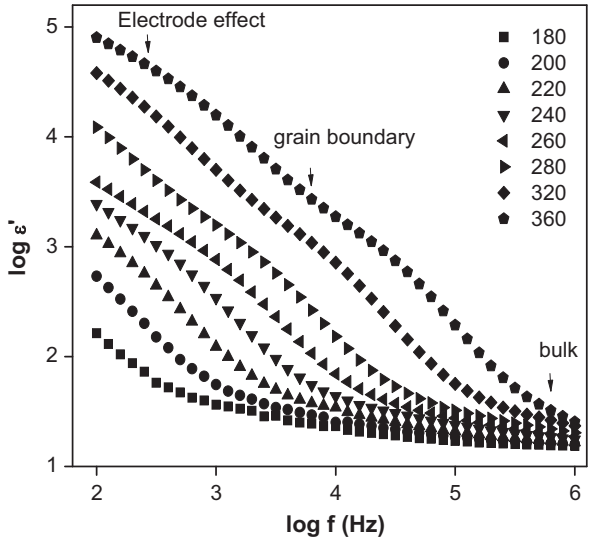

Fig. 5. Dielectric constant (ε') versus frequency for $Ce_{0.8}Y_{0.2}O_{1.9}$ sample at different temperatures (°C).

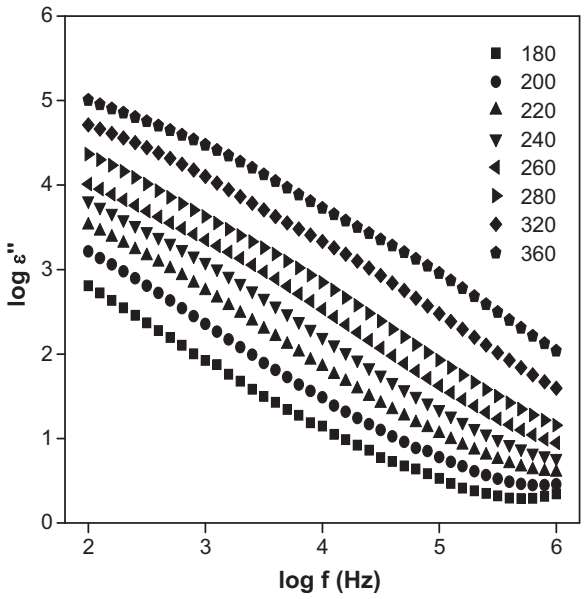

Fig. 6. Dielectric loss ε'' versus frequency for $Ce_{0.8}Y_{0.2}O_{1.9}$ sample at different temperatures (°C).

ity. The strong σ_{ac} dispersion in the intermediate frequency region observed in the sintered sample of yttria stabilized zirconia and is suggested due to the grain boundary resistivity [21], however the yttria doped zirconia single crystal which has no grain boundary also showed such a strong dispersion [22]. This fact suggests that the large dispersion obtained in the intermediate frequency range of the conductivity plot may also be due to the occurrence of mobile dimmer associates which do not participate in oxide ion conduction, but contribute to dielectric constant [23]. This means that the UDR theory could not always be appropriate in the case of oxide ion conductors.

The dielectric constant of oxide-ion conductors was composed of both Debye type polarization and electrode-electrolyte interfacial polarization which depends on the inverse of frequency [20]. The apparent dielectric constant (ε') can be given as in the following equation, assuming the presence of various dipoles with multiple relaxation times [24];

$$\varepsilon' = \varepsilon_\infty + \sum_i \frac{\varepsilon_{oi}}{1+(\omega\tau_{oi})^2} + \frac{\varepsilon(o)}{\omega^s} \quad (5)$$

where ε_{oi} and τ_{oi} represent the dielectric constant at low frequency limit due to the ith Debye type polarization and the ith dipole relaxation time respectively. $\varepsilon(o)$ is defined as the dielectric constant due to the interfacial polarization at low frequency limit, ε_∞ represent the dielectric constant at high frequency limit, frequency exponent s was introduced to generalize a function of frequency. The first two terms on the right hand side of Eq. (5) represent the Debye type dispersion, where $\varepsilon(o)$ in the second term was used in place of $\varepsilon(o)-\varepsilon_\infty$ in the usual Debye equation, because in the present case, $\varepsilon(o) \gg \varepsilon_\infty$. Fig. 5 shows frequency dependence of dielectric constant ε' at various temperatures. In the low frequency region, from 260° onwards an increase of ε' is attributed to the polarization of oxygen ions at the electrode–electrolyte interface. This behavior is quite common for the dielectric spectra of complex ionic conductors [7]. In the low frequency region, the ions jump in the field direction and pile up at sites with high free energy barrier resulting in an increase of capacitance in the field direction after successfully hopping through sites with low free energy barrier. At high frequencies, the periodic reversal of the field takes place so rapidly that there are no excess ion jumps in the field direction. The capacitive effect at high free energy barrier sites disappears, which reduces the contribution of charge carriers to the dielectric constant and is seen as a decrease in ε' with increase in frequency finally it saturates at higher frequencies giving rise to ε_∞ [25]. Figure shows the values of dielectric constant ε' increases and the dispersion at ε' is moving towards higher frequencies when the temperature increases. The dielectric dispersion observed at intermediate frequencies may be due to the grain boundary effect. Such dispersion at intermediate frequencies was also observed in Y doped ZrO_2 [22]. The variation of dielectric loss factor ε'' as a function of frequency at different temperature is shown in Fig. 6. It is supposed that ε'' includes a contribution of the conduction term ($\sigma_0/\omega\varepsilon_0$), in addition to Debye type dipole. The apparent ε'' can the expressed by the following equation,

$$\varepsilon'' = \sum_i \frac{\varepsilon_{oi}\omega\tau_{oi}}{1+(\omega\tau_{oi})^2} + \frac{\sigma_0}{\omega\varepsilon_o} \quad (6)$$

where the first term of the right hand side corresponds to Debye type polarization and σ_0 represent loss current conductivity at low frequency limit. The above equation suggests that the subtraction of $\sigma_0/\omega\varepsilon_0$ from ε'' value will only give the Debye-type relaxation peaks. The figure indicates that loss in dielectric constant is very high at low frequency region. This part comes from the free charges contributing to dc conduction and the bound charges which oscillate 90° out of phase with the applied time varying electric field [16]. According to dielectric theory, the activation energy of a dielectric relaxation process could be estimated from the dielectric loss factor ε''. However in the present oxide system, the loss factor did not give any dielectric relaxation process like many other oxide systems [8]. In such a case, the activation energy for the relaxation process is usually estimated by the approximation that the loss factor ε'' is proportional to the dielectric loss tangent $\tan\delta$ [9]. Fig. 7 shows the frequency dependence of dielectric loss tangent $\tan\delta$ at different temperatures. The $\tan\delta$ exhibit the presence of two distinct relaxation peaks at two resonant frequencies, one in the low frequency region ($f_{\tan\delta l}$) and another at high frequency region ($f_{\tan\delta h}$). Both relaxation peaks shifts to higher frequency region with increase in temperature, and an increase in the peak intensity at the same time. The fact that this spectrum contains two relaxation peaks is an important evidence for the relaxation due to ionic transport process of the bulk and the grain boundary [8,17,26].

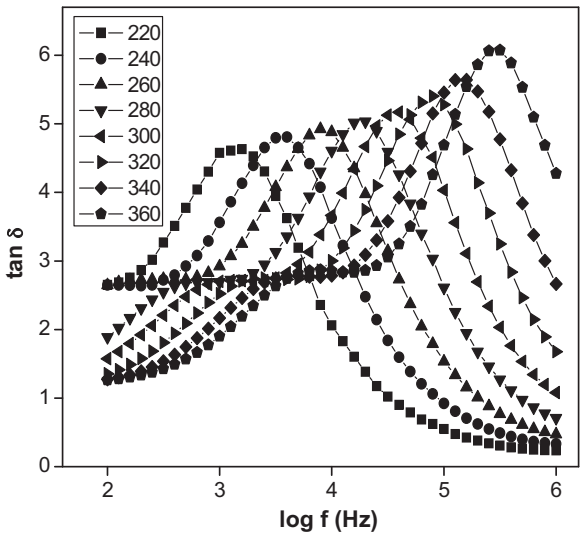

Fig. 7. Frequency dependence of tan δ at various temperatures.

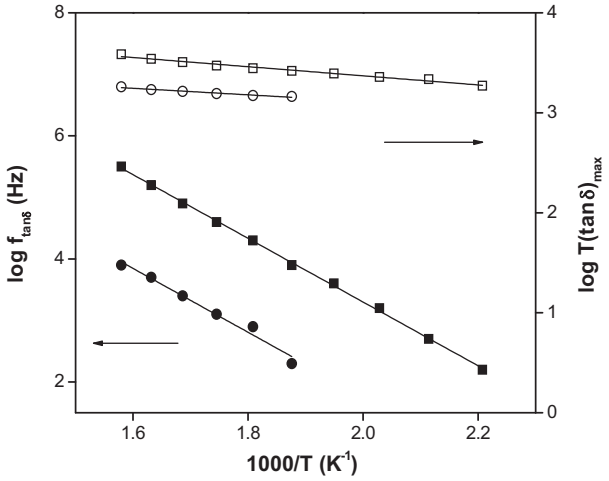

Fig. 8. Arrhenius relations of $\log f_{\tan\delta}$ vs. $1/T$ and $\log T(\tan\delta)_{max}$ vs. $1/T$; (■) and (□) for the high frequency peak and, (•) and (○) for the low frequency peak.

When CeO_2 is doped with yttria, one oxygen vacancy is introduced for every two Y^{3+} for charge neutrality. Each hop of an oxygen vacancy from one site to another leads to the orientation of dipole. When an electric field is applied, a portion of these dipoles become oriented in the field direction with a certain time delay, thus creating the frequency dependent polarization conductivity. The polarization conductivity is attributed to the dielectric relaxation, i.e., the non-cooperative or short range (localized) hopping motion of a charge carrier, such as an oxygen vacancy. This is different from the dc conductivity which involves frequency independent cooperative hopping motion. Usually, these oxygen vacancies will be associated with the dopant ions and in the conduction process the oxygen vacancies dissociate from the pairs and assist the migration of oxygen ions. The relaxation process resulting from the O^{2-} migration appears in the dielectric properties and their intensities are proportional to the number of migrating O^{2-} ions or the density of oxygen vacancies. For oxide electrolytes which contain excess oxygen vacancies, the oxygen vacancies get associated to the dopant ions at low temperatures and some energy is required to create a mobile vacancy. This is E_o, the dissociation energy of an oxygen vacancy from the restrained state. The activation energy for the dielectric relaxation process is the migration energy E_M associated with the jump of an O^{2-} ion, which requires ionic displacement around a saddle point in a diffusion path. The activation energy, E_a for oxygen ionic conduction is the sum of E_o and the migration energy E_M [19]. The Nernst–Einstein formula for the ionic conductivity due to oxygen ion migration is represented by $\sigma = 4e^2ND/k_BT$, where $4e^2$ is the square of the valence of an oxygen ion, and $D \propto \exp(-E_M/k_BT)$ is the diffusion co-efficient of O^{2-} ions, $N \propto \exp(-E_O/k_BT)$ is the density of the mobile free oxygen vacancies in thermal equilibrium because the assistance of vacancies is necessary in the O^{2-} diffusion, k_B is the Boltzmann constant [8,27]. In the present oxide system, where the dielectric relaxation process do not show up in the loss factor ε'', the activation energy is usually estimated by employing the approximation that the loss tangent is proportional to the loss factor, i.e., $\tan\delta \propto \varepsilon''$, then the maximum loss tangent has a form [8,9,11,22–29].

$$(\tan\delta)_{max} \propto \frac{\varepsilon_0 - \varepsilon_\infty}{2} \tag{7}$$

where ε_0 and ε_∞ are the static and high frequency dielectric constants. Since $(\varepsilon_0 - \varepsilon_\infty)T$ is proportional to the amount of migrating O^{2-} ions at T, i.e., the density of the free single oxygen vacancies at T, the above relation can be written as:

$$(\tan\delta)_{max} \propto N \propto \frac{\exp(-E_o/k_BT)}{T} \tag{8}$$

So the maximum value of the relaxation peak yield the energy required for the creation of oxygen vacancy assisting O^{2-} migration, E_O.

$$T(\tan\delta)_{max} \propto \exp\left(\frac{-E_o}{k_BT}\right) \tag{9}$$

The temperature dependence of the resonance frequency in tan δ gives the activation energy for the dielectric relaxation process and it is equal to the migration energy per oxide ion, E_M [8],

$$f_{\tan\delta} \propto \exp\left(\frac{-E_M}{k_BT}\right) \tag{10}$$

The binding energy or the association energy of the oxygen vacancies can be obtained from the Arrhenius plot of $\log(T\tan\delta_{max})$ versus $1/T$ plot. In the same way, the migration energy (E_M) associated with the jump of oxygen vacancies can be obtained from the Arrhenius plot of $\log(f_{\tan\delta})$ versus $1/T$ plot. Fig. 8 demonstrates the Arrhenius relation of $\log(f_{\tan\delta})$ vs $1/T$ and $\log[T(\tan\delta)_{max}]$ vs $1/T$ for the two peaks present at the tan δ plot. From the obtained straight lines we estimate the values of E_M = 1.02 eV and 1.03 eV, and E_O = 0.09 eV and 0.06 eV for the high and low frequency peaks. The sum of these energies is nearly equal to the activation energy obtained from the Arrhenius plot, $\log\sigma$ vs $1/T$, which is 1.05 eV and 1.09 eV for the bulk and grain boundary region. Sometime there is a difference of ~0.1 eV in the energy values obtained from the activation energy of conductivity plot and the tan δ plot [8]. Such difference is due to the difficulty in distinguishing the bulk and grain boundary contribution from the impedance analysis of the present system.

4. Conclusion

The dielectric dispersion studies of $Ce_{1.8}Y_{0.2}O_{1.9}$ system synthesized by mechanical milling technique were investigated in the temperature range from 140 to 360 °C. The ac conductivity σ_{ac} in the low frequency range was strongly influenced by space charge polarization at grain boundary and the high frequency plateau agreed with the bulk conductivity of the system at high temperatures. The dielectric relaxation process obtained from the ac conductivity studies provide detailed information of the bulk and

grain boundary contributions. The low frequency relaxation peak gives the idea about the grain boundary conduction and the high frequency peak resulting from the bulk conduction. The migration energy E_M and dissociation energy E_O for the O^{2-} migration has been obtained from the temperature dependencies of the resonance frequencies and the maximum values of these relaxation peaks. The sums of these two values are nearly equal to the activation energy obtained from the conductivity plot.

Acknowledgement

This work has been carried out with the financial support of Conacyt (Grant SEP-2007-CB-84267).

References

[1] T.H. Etsell, S.N. Flengas, Chem. Rev. 70 (1970) 339–376.
[2] R.G. Anderson, A.S. Nowick, Solid State Ionics 5 (1981) 547–550.
[3] J.A. Díaz-Guillén, M.R. Díaz-Guillen, K.P. Padmasree, A.F. Fuentes, J. Santamaría, C. León, Solid State Ionics 179 (2008) 2160–2164.
[4] D.K. Hohnke, Solid State Ionics 5 (1981) 531–534.
[5] D.S. Da Yu Wang, J. Park, A.S. Griffith, Nowick, Solid State Ionics 2 (1981) 95–105.
[6] R. Gerhardt, J. Phys. Chem. Solids 55 (1994) 1491–1506.
[7] A.K. Jonscher, J. Mater. Sci. 13 (1978) 553–562.
[8] E. Iguchi, S. Nakayama, F. Munakata, M. Kurumada, J. Appl. Phys. 93 (6) (2003) 3662–3664.
[9] M. Kurumada, H. Hara, E. Iguchi, Acta Mater. 53 (2005) 4839–4846.
[10] S. Komine, Solid State Ionics 178 (2007) 315–318.
[11] E. Iguchi, K. Ueda, W.H. Jung, Phys. Rev. B 54 (1996) 17431–17437.
[12] E. Iguchi, K. Akashi, J. Phys. Soc. Jpn. 61 (1992) 3385–3393.
[13] E. Iguchi, T. Hashimoto, S. Yokoyama, J. Phys. Soc. Jpn. 65 (1996) 221–229.
[14] S. Komine, F. Munukata, J. Mater. Sci. 40 (2005) 3887–3890.
[15] P. Sarkar, P.S. Nicholson, Solid State Ionics 21 (1986) 49–53.
[16] Mridula Biswas, J. Alloys Compd. 491 (2010) 30–35.
[17] Yi Liu, J. Alloys Compd. 479 (2009) 769–771.
[18] J. Li, T. Ikegami, Y. Wang, T. Mori, J. Solid State Chem. 168 (2002) 52–59.
[19] E. Iguchi, S. Mochizuki, J. Appl. Phys. 96 (2004) 3889–3895.
[20] H. Yamamura, H. Nishino, K. Kakinuma, J. Ceram. Soc. Jpn. 112 (10) (2004) 553–558.
[21] A. Pimenov, J. Ullrich, P. Lunkenheimer, A. Loidl, C.H. Ruscher, Solid State Ionics 109 (1998) 111–116.
[22] H. Yamamura, Y. Yagi, K. Kakinuma, J. Ceram. Soc. Jpn. 115 (9) (2007) 546–550.
[23] H. Yamamura, S. Takeda, K. Kakinuma, Solid State Ionics 178 (2007) 889–893.
[24] H. Yamamura, J. Satake, M. Saito, K. Kakinuma, Jpn. J. Appl. Phys. 47 (2008) 212–216.
[25] K.P. Padmasree, D.K. Kanchan, J. Non-Cryst. Solids 352 (2006) 3841–3848.
[26] S. Komine, Physica B 392 (2007) 348–352.
[27] M. Kurumada, H. Hara, F. Munakata, E. Iguchi, Solid State Ionics 176 (2005) 245–251.
[28] H. Fröhlich, Theory of Dielectrics Dielectric Constant and Dielectric Loss, Clarendon, Oxford, 1958.
[29] E.W. Iguchi, H. Jung, J. Phys. Soc. Jpn. 63 (1994) 3078–3086.